Title

ATP7A-dependent copper sequestration contributes to termination of β-CATENIN signaling during early adipogenesis.

Authors

Kabin, E
Dong, Y
Zhang, X
et al.

Publication Date

2024-01-06

DOI

10.1016/j.molmet.2024.101872

Peer reviewed

Original Article

MOLECULAR METABOLISM

ATP7A-dependent copper sequestration contributes to termination of β-CATENIN signaling during early adipogenesis

H. Yang[1,**], E. Kabin[2,3,5], Y. Dong[3,5], X. Zhang[3], M. Ralle[4], S. Lutsenko[3,*]

ABSTRACT

Objectives: Adipocyte fate determination is tightly regulated by extrinsic signaling pathways and intrinsic metabolic and morphologic changes that maintain adipose tissue function. Copper (Cu) homeostasis is required for the normal metabolism of mature adipocytes, whereas the role of Cu in adipogenesis is unclear.

Methods: To determine the role of Cu is adipocytes differentiation, we used 3T3-L1 adipocytes, immunocytochemistry, X-ray fluorescence, mass-spectrometry, pharmacological treatments, and manipulations of copper levels.

Results: In differentiating 3T3-L1 cells, adipogenic stimuli trigger the upregulation and trafficking of the Cu transporter Atp7a, thus causing Cu redistribution from the cytosol to vesicles. Disrupting Cu homeostasis by the deletion of Atp7a results in Cu elevation and inhibition of adipogenesis. The upregulation of *C/EBPβ*, an initial step of adipogenesis, is not affected in *Atp7a*$^{-/-}$ cells, whereas the subsequent upregulation of *PPARγ* is inhibited. Comparison of changes in the *Atp7a*$^{-/-}$ and wild type cells proteomes during early adipogenesis revealed stabilization of β-catenin, a negative regulator of adipogenesis. Cu chelation, or overexpression of the Cu transporter ATP7B in *Atp7a*$^{-/-}$ cells, restored β-catenin down-regulation and intracellular targeting.

Conclusions: Cu buffering during early adipogenesis contributes to termination of β-catenin signaling. Abnormal upregulation of β-catenin was also observed *in vivo* in the livers of *Atp7b*$^{-/-}$ mice, which accumulate Cu, suggesting a tissue-independent crosstalk between Cu homeostasis and the Wnt/β-catenin pathway. These results point to a new regulatory role of Cu in adipocytes and contribute to better understanding of human disorders of Cu misbalance.

Keywords Copper; Adipocytes; ATP7A; β-catenin

1. INTRODUCTION

Copper (Cu) has a multifaceted role in mammalian physiology and is essential for normal development and function of humans, animals, and many other species. The best-known function of Cu is to serve as a cofactor of important metabolic enzymes, such as cytochrome c oxidase, superoxide dismutases SOD1 and SOD3, amino-oxidase AOC3 and many others [1]. It is now appreciated that Cu is also an important regulator of kinase-mediated signaling, autophagy, and even cell death [2–5]. Either Cu deficiency or Cu overload is harmful to cells. Consequently, cells faithfully maintain Cu homeostasis using Cu transporting proteins, which ensure proper and timely Cu distribution to the intracellular compartments. Cu uptake is mediated primarily by SLC31A1 (CTR1), whereas the ATP-driven transporters ATP7A (Atp7a in mice) and ATP7B transport Cu into the secretory pathway to activate Cu-dependent enzymes and lower cytosolic Cu by exporting excess Cu into vesicles and eventually out of cells [6]. ATP7A and ATP7B are highly homologous, and both play critical roles in regulation of cellular Cu levels. Inactivation of either ATP7A or ATP7B is associated with debilitating and even fatal diseases [7].

Recently, the new role for ATP7A in cell differentiation was identified. Expression of ATP7A was found to change during neuronal differentiation [5,8], and was associated with a transient decrease in the cellular Cu levels [9]. Loss of ATP7A function in neurons causes defects in their axon outgrowth and synaptogenesis [10]. Cu is required for myogenesis (during which ATP7A is significantly upregulated [11]), for spermatogenesis (where changes in the expression of ATP7A, ATP7B, and CTR1 occur at different steps of sperm maturation [12]), and for angiogenesis (neovascularization [13]). However, understanding of how Cu is used during cell differentiation remains very limited.

[1]Helen Diller Family Comprehensive Cancer Center, University of California, San Francisco, CA, USA [2]Department of Chemistry and Biotechnology, Tallinn University of Technology, Akadeemia tee 15, 12618 Tallinn, Estonia [3]Department of Physiology, Johns Hopkins Medical Institutes, Baltimore, MD, USA [4]Department of Molecular Genetics, OHSU, Portland OR, USA

[5] Kabin E. and Dong Y. contributed equally to this work.

*Corresponding author. E-mail: lutsenko@jhmi.edu (S. Lutsenko).

**Corresponding author. E-mail: haojun.yang@ucsf.edu (H. Yang).

Received December 4, 2023 • Accepted January 3, 2024 • Available online 6 January 2024

https://doi.org/10.1016/j.molmet.2024.101872

Cu homeostasis is required for normal functions of adipose tissue [14—16], but the role of ATP7A in adipogenesis remains unclear. In mice, targeted deletion of *Atp7a* gene in adipocytes is associated with Cu elevation, age-dependent atrophy and diminished function of white adipose tissue. This is evident from the lower levels of serum leptin and adiponectin, elevated serum triglycerides, and hepatic steatosis [17]. It is unknown whether these abnormalities reflect defects in adipocytes differentiation or the toxicity of elevated Cu in fully differentiated cells. Studies of adipocytes differentiation in animals are complicated by complex interactions with other cell types [18,19]. Consequently, to better understand the role of Cu homeostasis in adipocytes, we used 3T3-L1 mouse preadipocytes, an established model for adipocyte differentiation. We found that Atp7a-dependent Cu distribution is required for early steps of 3T3-L1 adipocytes differentiation and identified a new role for Cu in sustaining Wnt/β-catenin signaling, a conserved pathway that regulates cell proliferation and differentiation. We demonstrated that the adipogenic stimuli alter the intracellular Cu distribution by affecting Atp7a abundance and localization, and that without this regulation the Wnt/β-catenin is prolonged and adipogenesis is impaired. Moreover, we showed that Cu accumulation leads to stabilization of β-catenin in an animal model of Wilson disease, which points to a new mechanism through which Cu can contribute to the development of human pathologies.

2. RESULTS

2.1. Atp7a-dependent Cu distribution changes during adipogenesis

To understand the role of Cu homeostasis in functional maturation of 3T3-L1 adipocytes, we first examined the expression status of major Cu transporters: Atp7a, Atp7b, and Slc31a1 (Ctr1) during a standard 8-day differentiation process [20]. Immunoblotting revealed that Atp7a was present in differentiated adipocytes, whereas Atp7b was not (Figure 1A). Furthermore, the expression of Atp7a protein was significantly higher in fully differentiated adipocytes than in pre-adipocytes (Figure 1B). Quantitative PCR on different differentiation time points demonstrated that upregulation of *Atp7a* mRNA occured early in differentiation, right after the growth arrest, and was associated with the increased Atp7a protein levels on day 3 of differentiation (Figure 1C—E). By contrast, the expression of *Ctr1* did not change at the early stage of differentiation, but was upregulated at the later stage, on day 6 (Figure 1F).

In adipocytes, Atp7a transfers Cu to Cu-dependent enzymes, such as Aoc3 [21]. This process takes place in the *trans*-Golgi network (TGN). Atp7a also lowers cytosolic Cu levels by sequestering Cu into vesicles and exporting Cu via plasma membrane [6]. In either mature or non-differentiated adipocytes, Cu limitation facilitates Atp7a retention in the TGN, whereas high Cu triggers Atp7a movement from the TGN to vesicles, in agreement with its known regulation in other cell types (Suppl. Fig. 1A,B). Analysis of Atp7a localization during adipogenesis revealed that the balance between the two Atp7a functions (TGN delivery and vesicular Cu sequestration/export) changed as adipocytes differentiate. In preadipocytes, Atp7a was found mainly in the TGN (Figure 1F). On day 3 of differentiation (D3), Atp7a was upregulated and trafficked from the TGN to vesicles (Figure 1D,G and Suppl. Fig. 2A,B) and towards the plasma membrane, which indicated increased Cu sequestration and export. On day 5, Atp7a mostly returned to the TGN, with only a small amount detected in vesicles. The fully mature adipocytes (day 8) had Atp7a in the TGN (Figure 1F). Considering that the *Ctr1* levels (and hence Cu uptake) increased only on day 6 of differentiation (Figure 1F), the earlier upregulation and vesicular targeting of Atp7a suggest that the initial steps of adipogenesis may require lowering of cytosolic Cu.

We also tested whether insulin, the major component of adipogenic cocktail, alone triggers Atp7a trafficking and whether this process is copper dependent. We examined Atp7a localization in 3T3-L1 cells treated with TTM (an intracellular copper chelator), and TTM followed by insulin (Suppl. Fig. 2C). Insulin alone (without other components of differentiation cocktail) induced trafficking of Atp7a from the TGN to vesicles even when Cu was chelated (Suppl. Fig. 2C). Taken together, these results show that Atp7a-dependent intracellular Cu redistribution is an integral component of the adipogenesis program.

2.2. Deletion of Atp7a alters the intracellular Cu redistribution and inhibits adipogenesis at the early stage

To further examine significance of Atp7a function in adipocyte differentiation, we used 3T3-L1-*Atp7a*$^{-/-}$ cells, previously generated using CRISPR/Cas9. These cells lack the Atp7a-dependent Cu export and accumulate Cu ([22,23], Figure 1D and Suppl. Figure 3A). We first examined the intracellular Cu distribution using X-ray fluorescence imaging (Figure 2A), an analytical technique that allows direct and quantitative analysis of various elements, including Cu, in cells and tissues with high sensitivity and specificity [21,24,25]. Phosphate, an integral component of nucleic acids thus enriched in the nuclei, was served as a control. As expected, the levels and compartmentalization of phosphate were similar for control and *Atp7a*$^{-/-}$ cells. In contrast, Cu distribution changed. In wild-type (WT) cells Cu was enriched in the perinuclear area, and Cu levels in the nuclei were low (Figure 2A). In *Atp7a*$^{-/-}$ cells, Cu levels were increased throughout the cell including the nuclei (Figure 2A). We also found that *Atp7a*$^{-/-}$ cells proliferated slower than control 3T3-L1 cells. The lower proliferation rate is likely caused by the defects in a cell cycle progression, as we found no increase in cell death (Suppl Fig. 3B). Further analysis demonstrated that not only cells grew slower, but the differentiation of 3T3-L1-*Atp7a*$^{-/-}$ cells into functional adipocytes was inhibited. At the end of the differentiation program, *Atp7a*$^{-/-}$ cells remained flat and contained fewer and smaller lipid droplets than the WT cells (Figure 2B). The Oil red O staining that detects triglycerides and cholesteryl esters confirmed a paucity of lipid droplets in differentiated *Atp7a*$^{-/-}$ cells (Figure 2B). In agreement with the staining data, total triglyceride levels were significantly lower in 3T3-L1 *Atp7a*$^{-/-}$ cells compared to 3T3-L1 controls (Figure 2C).

To verify that these changes were caused by the loss of Atp7a function and were not the off-target effects of CRISPR/Cas9, we generated an additional 3T3-L1-based cell line using shRNA, wherein Atp7a was down-regulated by approximately 70% (Suppl. Fig. 3C). These Atp7a knockdown cells had altered cell morphology (Suppl. Fig. 2D), accumulated Cu (Suppl. Fig. 2E), had a slower growth rate, and diminished adipogenic differentiation (Suppl. Fig. 2F,G). In other words, their key characteristics were very similar to *Atp7a*$^{-/-}$ cells. Taken together, the data suggest that Atp7a is required, in some capacity, for pre-adipocytes transitioning to mature adipocytes.

Adipogenesis is controlled by a balance of internal and external factors, which either stimulate or repress cells differentiation. During the early phase of adipocytes differentiation, CCAAT/enhancer binding proteins C/EBPβ and C/EBPδ induce the expression of C/EBPα and PPARγ [26], the principal transcription factors that control early differentiation of preadipocytes into mature lipid-accumulating cells. The qPCR analysis of *C/EBPβ* and *C/EBPδ* mRNA revealed that both were upregulated in WT cells 24 h after induction of differentiation, as expected (Figure 2D,F). In *Atp7a*$^{-/-}$ cells 24 h after induction of differentiation, *C/EBPβ* mRNA levels were comparable to WT and *C/EBPδ* mRNA levels were even higher (Figure 2D,E). Thus, this step of differentiation

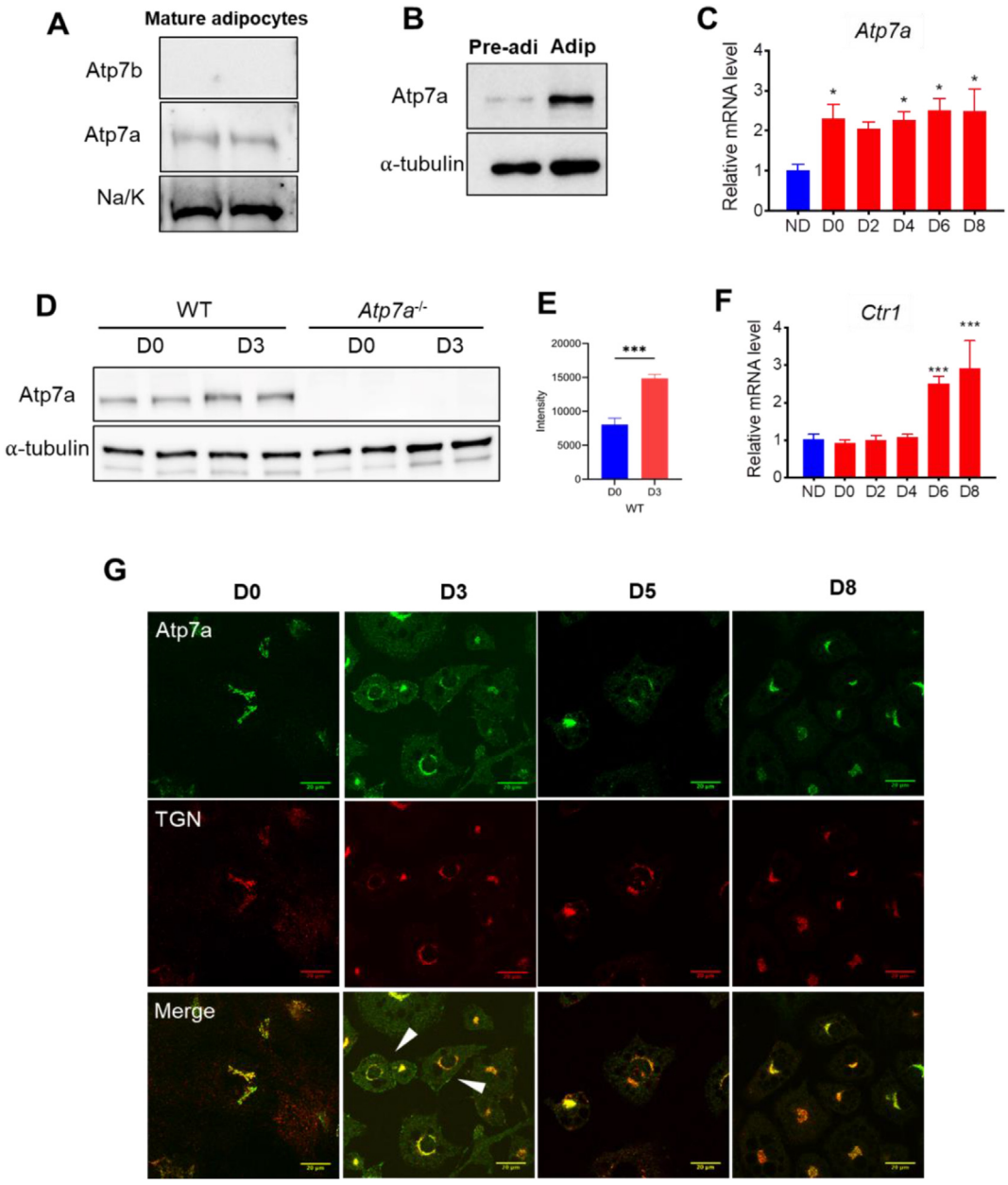

Figure 1: Cu transporter Atp7a upregulates and relocates during adipogenesis. (A) Immunoblot of Atp7a and Atp7b in differentiated 3T3-L1 adipocytes on day 8. **(B)** Protein levels of Atp7a in pre-differentiated (pre-Adi), differentiated adipocytes (Adip). **(C)** Relative mRNA levels of *Atp7a,* normalized to non-differentiated cells (ND) ($n = 3$). **(D)** Immunoblot of Atp7a in 3T3-L1 cells in early differentiation day 3 after adipogenic stimuli and **(E)** associated quantifications. **(F)** Relative mRNA levels of *Ctr1* in pre-adipocytes, on day 0, day 2, day 4, day 6, and day 8 after adipogenic stimuli, normalized to the levels in preadipocytes ($n = 3$). **(G)** Immunostaining of Atp7a (green) and TGN marker (syntaxin 6, red) in pre-adipocytes, on day 0, day 3, day 5, and day 8 after adipogenic stimuli. All values represent the mean ± SEM; One-way ANOVA was used to analyze the data in C and F, Student t-test was used for E. $^{*} - p < 0.05$, $^{***} - p < 0.001$.

appears to be largely independent of Atp7a activity. In contrast, on day 3 (D3), when the abundance and localization of Atp7a changes significantly in WT cells, the mRNA levels of *C/EBPα* and *Pparγ* in *Atp7a*$^{-/-}$ cells were markedly lower than in controls. The WT cells had *C/EBPα* and *Pparγ* upregulated by more than 50-fold relative to day 0, whereas *Atp7a*$^{-/-}$ cells had only modest upregulation of *C/EBPα* and very little upregulation of *Pparγ* (Figure 2F). These changes in the expression of key differentiation factors suggest that the Atp7a activity is critical for the differentiation step(s) after the *C/EBPβ* and *C/EBPδ* induction, and that the loss of Atp7a inhibits signaling that results in the activation of *C/EBPα* and *Pparγ*.

2.3. Inactivation of Atp7a leads to specific changes in 3T3-L1 cells proteome

To identify signaling pathways that were altered in *Atp7a*$^{-/-}$ cells, we compared changes in proteomes of WT 3T3-L1 cells and two clonal lines of *Atp7a*$^{-/-}$ cells during the day0-to-day3 (D0-D3) transition using TMT-labelling mass-spectrometry (Figure 3A). Changes in protein abundance showed that during D0-D3 transition WT cells increased fatty acid oxidation, fatty acid synthesis, and proteins involved in lipid storage (Figure 3B). The RhoA and actin cytoskeleton signaling were decreased, and the processes leading to osteoclast differentiation were inhibited (Figure 3B). When the proteome of

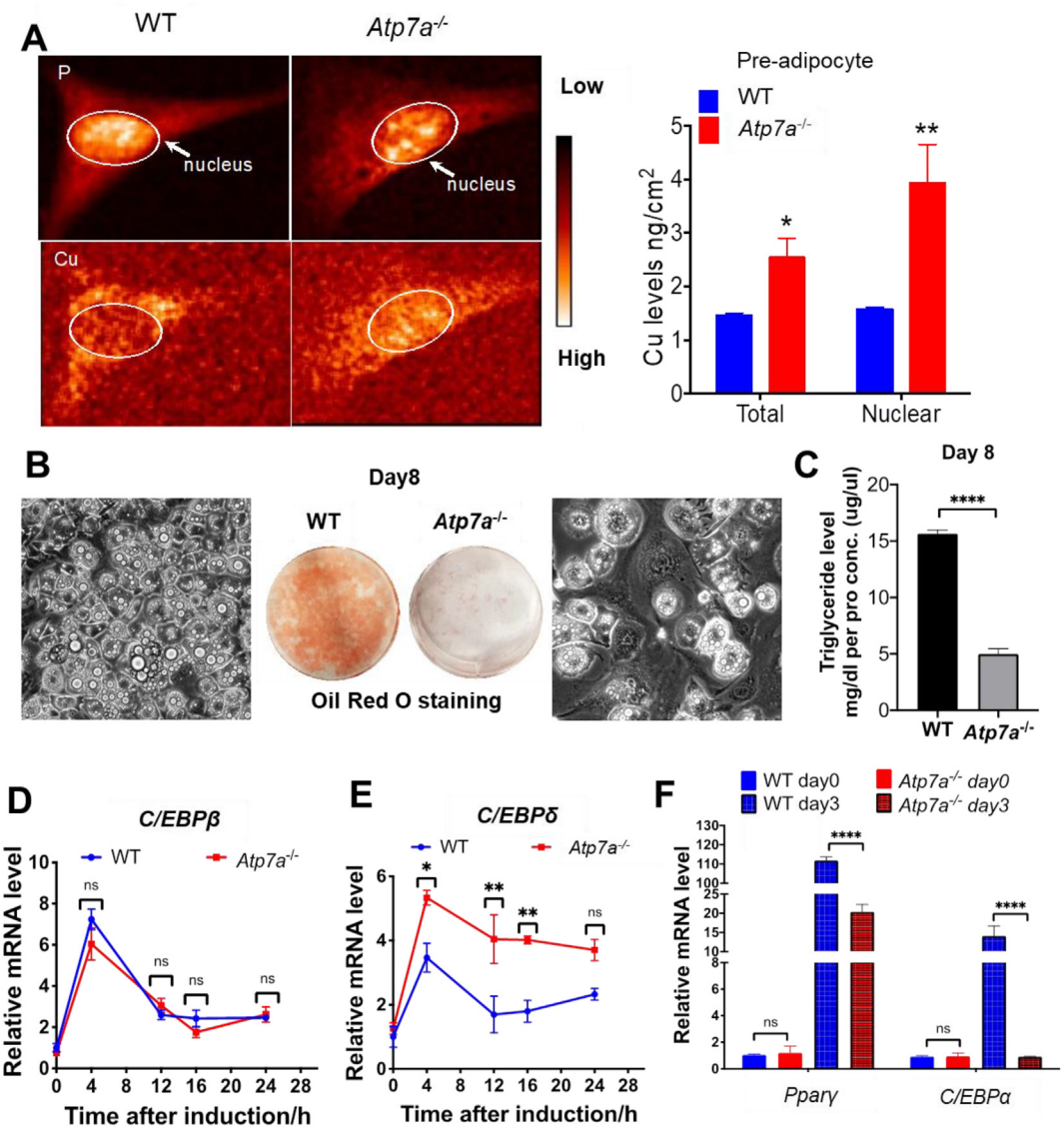

Figure 2: Atp7a inactivation is associated with changes in Cu distribution, cell morphology and inhibition of adipogenesis. (A) X-ray fluorescence imaging and quantification of Cu in control (WT) and *Atp7a*$^{-/-}$ pre-adipocytes. Signal of phosphate (P) serves as an abundant internal control and identification of the nucleus in cells. **(B)** Representative images of cell morphology and oil red O stained differentiated WT and *Atp7a*$^{-/-}$ 3T3-L1 adipocytes on day 8 (n = 3). **(C)** Relative triglyceride content in differentiated WT and *Atp7a*$^{-/-}$ 3T3-L1 adipocytes on day 8 (n = 3). **(D)** Relative mRNA levels of *C/EBPβ* and **(E)** *C/EBPδ* in WT and *Atp7a*$^{-/-}$ cells during the first 24 h following stimulation of adipogenesis, normalized to WT cells at time 0 (n = 3). **(F)** Relative mRNA levels of *PPARγ* and *C/EBPα* in *Atp7a*$^{-/-}$ cells on day 0 and day 3, normalized to WT cells on day 0 (n = 3). All values represent the mean ± SEM. Student t -est was used for C and two-way ANOVA have been used for A, D, E and F; ns — $p > 0.05$, * — $p < 0.05$, ** — $p < 0.01$, **** — $p < 0.0001$.

Atp7a$^{-/-}$ cells was compared to WT on D3, main differences included an increased cell spreading with a formation of protrusions (p-value 5.48×10^{-18}, z-core 4.184, Figure 3C). Indeed, *Atp7a*$^{-/-}$ cells were larger and more flattened comparing to WT cells, as shown by α-tubulin staining (Figure 3D). Proteins associated with osteoclasts differentiation were upregulated in *Atp7a*$^{-/-}$ cells along with a diminished metabolism of triglycerides (Figure 3C). Taken together, these results point to an early differentiation defect in *Atp7a*$^{-/-}$ cells.

To identify proteins most significantly associated with the adipogenesis defects in *Atp7a*$^{-/-}$ cells, we focused on the genes that were highly changed upon adipogenic stimuli in WT cells by using a 4-fold cut-off (Figure 3E). Then we compared the expression of those genes in WT and *Atp7a*$^{-/-}$ cells using the cluster function in Heatmap.2 R package (this function uses euclidean measure to obtain distance matrix and complete agglomeration method for clustering). This approach identified the group of proteins that showed the largest difference between the WT and *Atp7a*$^{-/-}$ cells during D0-D3 transition (Figure 3E). Proteins in this group were markedly down-regulated in WT cells on D3 compared to D0, but failed to decrease in *Atp7a*$^{-/-}$ cells during the same period. This group included β-catenin, a well-known inhibitor of adipogenesis.

β-catenin is a key component of the canonical Wnt/β-catenin signaling pathway; the translocation of β-catenin to the nucleus is associated with the inhibition of C/EBPα and PPARγ expression [27]. On D3, β-catenin was significantly down-regulated in WT, which differentiated successfully, whereas the *Atp7a*$^{-/-}$ cell lines maintained a fairly high

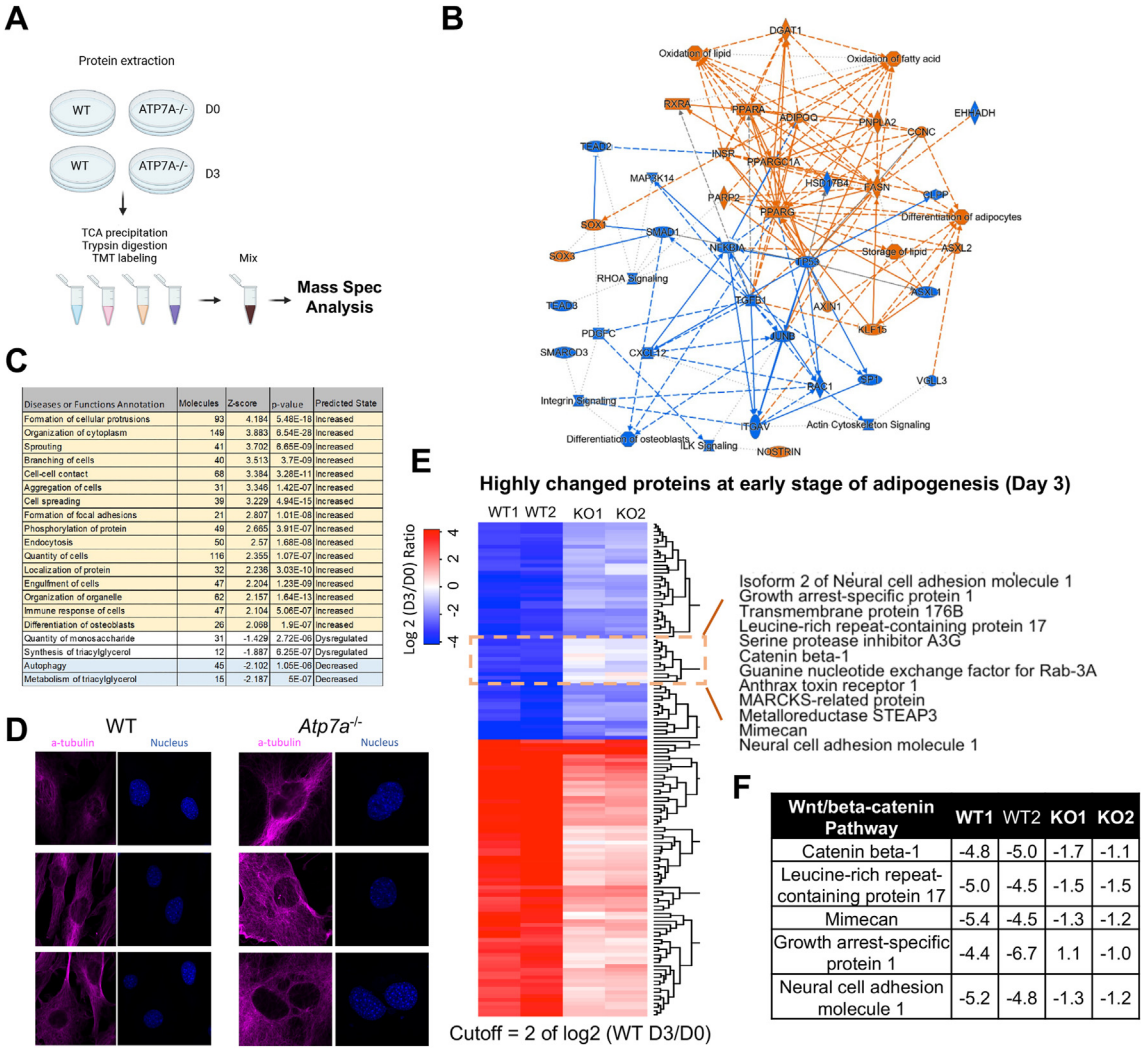

Wnt/beta-catenin Pathway	WT1	WT2	KO1	KO2
Catenin beta-1	-4.8	-5.0	-1.7	-1.1
Leucine-rich repeat-containing protein 17	-5.0	-4.5	-1.5	-1.5
Mimecan	-5.4	-4.5	-1.3	-1.2
Growth arrest-specific protein 1	-4.4	-6.7	1.1	-1.0
Neural cell adhesion molecule 1	-5.2	-4.8	-1.3	-1.2

Figure 3: Analysis of WT and *Atp7a*$^{-/-}$ 3T3-L1 cells proteomes during early differentiation. (A) Schematic overview of TMT labeling mass spectrometry. **(B)** Summary of processes primarily changed in 3T3-L1 cells during day0-day3 transition: orange — upregulated, blue down-regulated. **(C)** Major functional differences between the 3T3-L1 and *Atp7a*$^{-/-}$ cells on day 3. **(D)** Immunostaining of α-tubulin in WT and *Atp7a*$^{-/-}$ 3T3-L1 preadipocytes. **(E)** Heatmap of highly changed proteins in WT 3T3-L1 during early adipogenesis stage, the cutoff used is 4-fold change. Clustering function in Heatmap.2 package. The box area is the list indicates the least down-regulated genes in *Atp7a*$^{-/-}$ cells compared to control adipocytes; β-catenin is among these least down-regulated proteins. **(F)** Table of $\log_2$ fold change in abundance for proteins involved in Wnt/β-catenin pathway during D0-D3 transition.

level of β-catenin (Figure 3E). Several other proteins involved in Wnt/β-catenin pathway were also decreased by more than 16-fold in WT at D3 but showed only a mild decrease in *Atp7a*$^{-/-}$ cells (Figure 3F). These differences in the proteomes suggest that *Atp7a*$^{-/-}$ cells do not properly down-regulate the Wnt/β-catenin signaling pathway, which in turn may block adipogenesis.

2.4. Elevated Cu stabilizes Wnt/β-catenin signaling *in vitro* and *in vivo*

To test whether *Atp7a*$^{-/-}$ cells have sustained β-catenin signaling, we further investigated expression of the Wnt/β-catenin pathway members. Wnt ligands, such as Wnt10 b, Wnt10a and Wnt6, which activate the Wnt pathway and stabilize β-catenin protein levels, have been shown to inhibit adipogenesis [28]. In *Atp7a*$^{-/-}$ cells on D3 of adipogenesis, the mRNA levels of *Wnt10*, and *Wnt6* were significantly higher compared to WT 3T3-L1 cells (Figure 4A). *Wnt10b* showed the most significant increase, being upregulated by 2.5-fold (Figure 4A). Western blot analysis of β-catenin confirmed the mass-spectrometry findings, showing the decline of β-catenin' expression on D3 in WT cells but not in *Atp7a*$^{-/-}$ cells (Figure 4B).

Normally, degradation of β-catenin is initiated by phosphorylation of several Ser/Thr sites by GSK3 kinase [29]. Wnt signaling decreases phosphorylation of β-catenin, which leads to stabilization of β-catenin and its trafficking to the nucleus for activation of downstream targets. Western blot analysis of cells lysates demonstrated that elevated Cu did not affect Gsk-3α/β levels (Figure 4B), but decreased its activity: i.e. phosphorylation of β-catenin in *Atp7a*$^{-/-}$ cells was lower compared to WT, in agreement with the observed β-catenin stabilization (Figure 4B). To test whether stabilization of β-catenin enhances its trafficking into the nucleus, we immunostained the WT and *Atp7a*$^{-/-}$ cells and found a strong nuclear localization of β-catenin in *Atp7a*$^{-/-}$ cells, but not in WT cells on D3, consistent with a prolonged β-

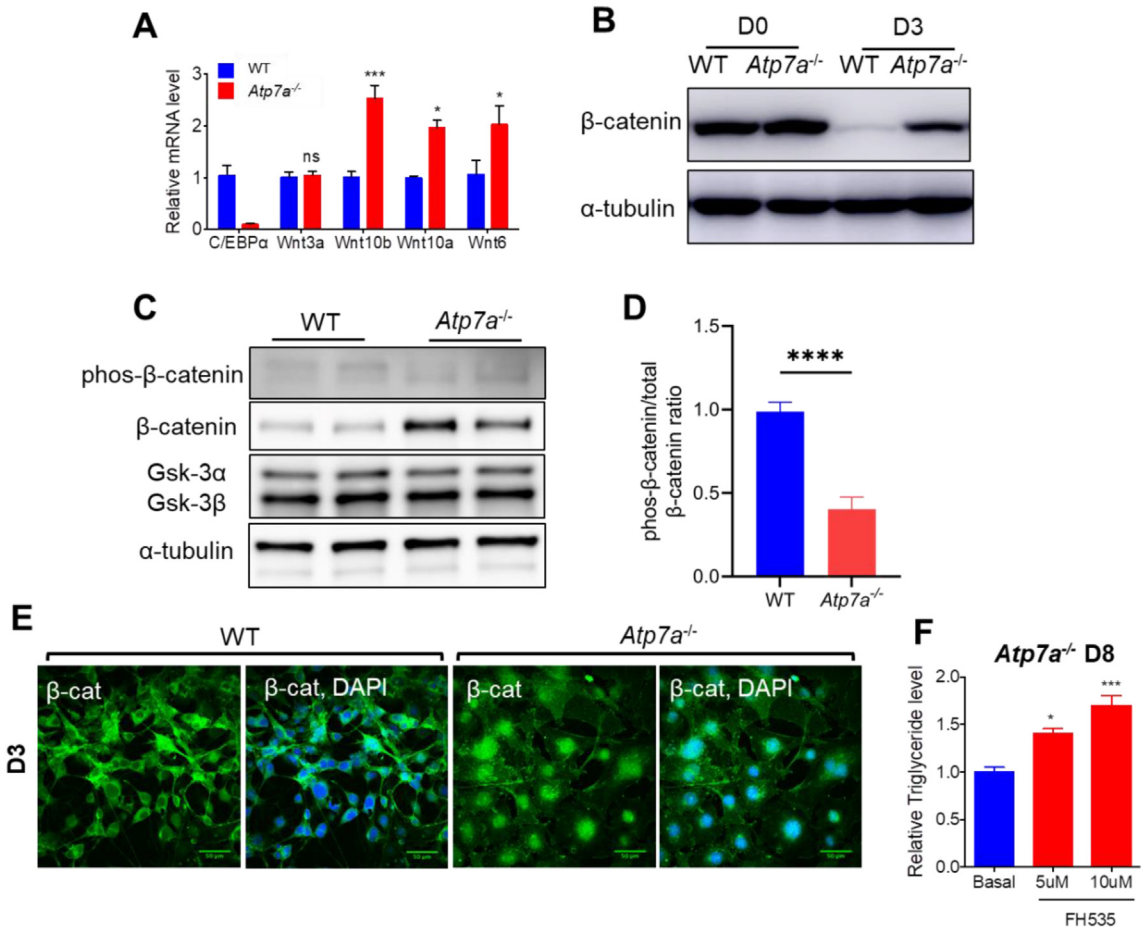

Figure 4: Wnt/β-catenin signaling persists in Cu overloaded cells during adipogensis. (A) Relative mRNA levels of *C/EBPα*, *Wnt10b*, *Wnt10a* and *Wnt6* in *Atp7a*$^{-/-}$ 3T3-L1 normalized to WT cells on day 3 (n = 3). **(B)** Immunoblot of β-catenin in WT and *Atp7a*$^{-/-}$ 3T3-L1 cells on day 0 and day 3, α-tubulin was used as internal control. **(C)** Immunoblot of β-catenin, phosphorylated-β-catenin, and Gsk3 in WT and *Atp7a*$^{-/-}$ 3T3-L1 cells on day 3 and quantification for **(D)** phosphorylation levels of β-catenin. **(E)** Immunostaining of β-catenin (green) and DAPI (blue) in WT and *Atp7a*$^{-/-}$ 3T3-L1 cells on day 3 after differentiation stimuli. **(F)** Relative triglyceride levels in differentiated *Atp7a*$^{-/-}$ cells (day 8) in either basal medium or medium containing 5 μM or 10 μM of the β-catenin inhibitor FH535 from day0 to day 3 during adipogenesis (n = 3). All values represent the mean ± SEM. Student t test was used for D, One-way ANOVA was used for F and two-way ANOVA was used for A. ns − $p > 0.05$ * − $p < 0.05$, *** − $p < 0.001$.

catenin signaling (Figure 4C). Finally, to examine whether this altered Wnt/β-catenin signaling contributes to defective adipogenesis, we treated *Atp7a*$^{-/-}$ cells with FH535, an inhibitor of Wnt/β-catenin signaling, during the D0-D3 differentiation step. FH535 treatment increased the triglyceride content in *Atp7a*$^{-/-}$ cells (Figure 4D) in agreement with an improved adipogenesis.

2.5. Cu-dependent redox misbalance contributes to β-catenin stabilization

The elevation of Cu in either *Atp7a*$^{-/-}$ skin fibroblasts or adipocytes was previously shown to induce oxidative stress [22,23]. Consequently, we tested whether normal 3T3-L1 cell differentiation is accompanied by changes in redox balance, i.e. whether this redox misbalance can contribute to defects in adipogenesis. Using roGFP-Grx1 sensor, we found that during D0-D3 transition the control (WT) 3T3-L1 cells maintained their redox status (Figure 5A,B) in the cytosol, and their cytosol and nucleus were more reducing than the *Atp7a*$^{-/-}$ cytosol, as evident by higher oxidation of roGFP-Grx1 sensor in *Atp7a*$^{-/-}$ cells (Figure 5C,D). To test whether this increased oxidation can contribute to β-catenin stabilization, we treated *Atp7a*$^{-/-}$ cells with N-acetyl cysteine, a well-known antioxidant. We found that this treatment rescued β-catenin degradation in a dose-dependent manner (Figure 5E).

2.6. Cu levels modulate both the stability and intracellular targeting of β-catenin

Finally, to test whether the *Atp7a*$^{-/-}$ phenotype can be rescued by restoring Cu transport to secretory pathway, we overexpressed human Cu transporter ATP7B in *Atp7a*$^{-/-}$ cells, which also sequesters excess Cu in the secretory pathway and decreases Cu in the cytosol. This overexpression increased levels of triglycerides in *Atp7a*$^{-/-}$ cells after adipogenic stimuli, indicative of better adipogenesis (Figure 6A). Significantly, overexpression of human ATP7B dramatically decreased β-catenin staining in the nuclei (Figure 6B), as well as the total abundance of β-catenin (Figure 6C). Overexpression of ATP7B-D1027A mutant, which cannot export Cu, had no effect on the β-catenin levels in *Atp7a*$^{-/-}$ cells on D3 (Figure 6C). Taken together, these results strongly suggest that elevated cellular Cu is the key factor that induces accumulation of β-catenin and β-catenin targeting. This was further supported by our observation that Cu chelator BCS rescued

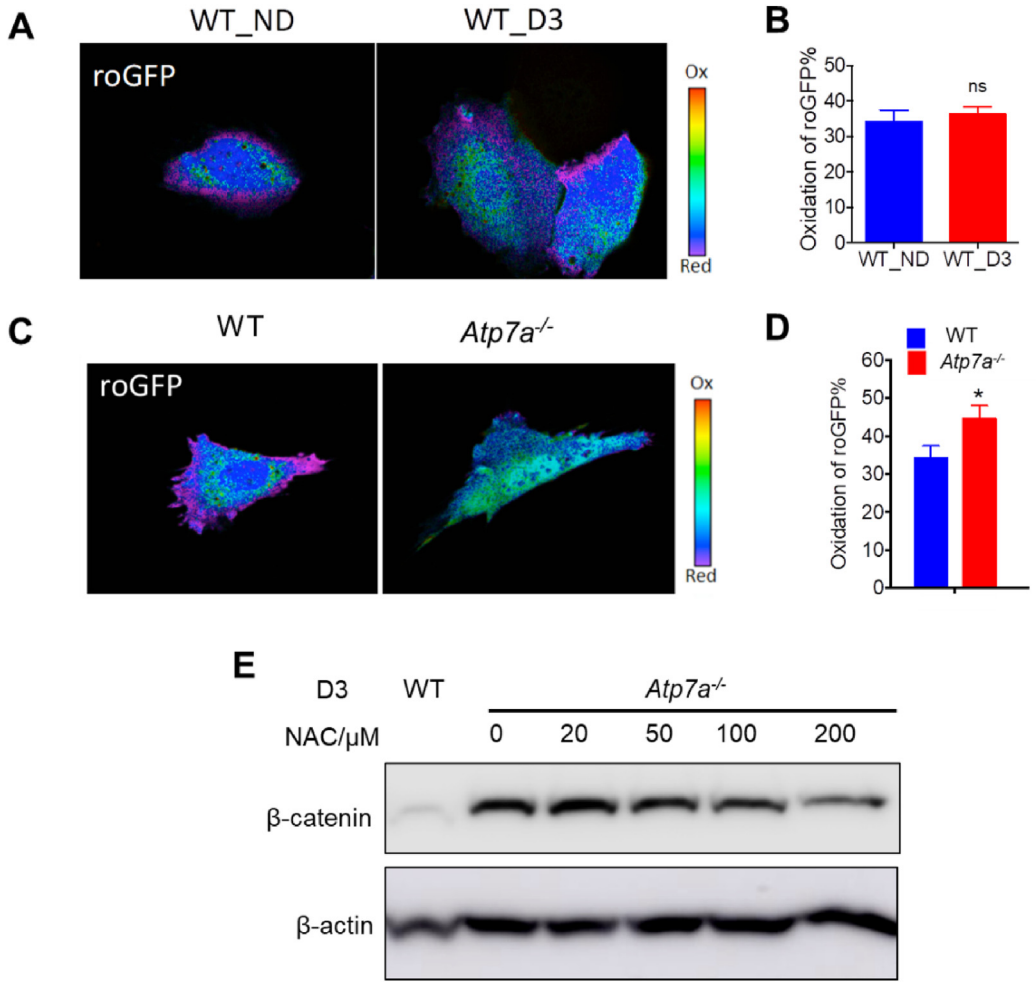

Figure 5: Different redox environment in control (WT) and *Atp7a*$^{-/-}$ cells contributes to different β-catenin stability. (A) Ratiometric representation and **(B)** quantification of Grx-roGFP signal in cytosol of non-differentiated WT cells (WT_ND) and WT cells on day 3 after differentiation stimuli (n = 38). **(C)** Ratiometric representation and **(D)** quantification of Grx-roGFP signal in cytosol in control (WT) and *Atp7a*$^{-/-}$ 3T3-L1 cells (n = 24). **(E)** Western blot of β-catenin on day 3 after stimulation treated with different concentration of NAC, β-actin was used as internal control. All values represent the mean ± SEM. Student t-test was used for B and D. ns − $p > 0.05$ * − $p < 0.05$.

the downregulation of β-catenin levels in a dose-dependent manner (Figure 6D).

Finally, we tested whether the Cu-dependent stabilization of β-catenin is unique to *Atp7a*$^{-/-}$ adipocytes or copper elevation may have a similar effect in other cells or tissues. *Atp7b*$^{-/-}$ mice, a mouse model of Wilson disease, accumulate copper in the liver to high levels [30]. We found that the hepatic abundance of β-catenin was significantly increased in *Atp7b*$^{-/-}$ mice compared to WT (Figure 6E). Altogether, these results confirm a stabilizing effect of elevated Cu on β-catenin signaling.

3. DISCUSSION

In this study, we investigated the role of Cu during 3T3-L1 adipocyte differentiation and identified a Cu-dependent step in the early adipogenesis program, and a new role for excess Cu in prolonging the Wnt/β-catenin signaling. It was previously demonstrated that the expression of Cu transporters, such as ATP7A, changes upon cell differentiation [11]. However, functional significance of this change has not always been apparent. Taken together, our data suggest that the Atp7a-dependent decrease of cytosolic Cu during early adipogenesis allows for better control of intracellular redox balance, enhanced degradation of cytosolic β-catenin, and stabilization of cytoskeletal elements, thus fine-tuning both transcriptional and morphogenic functions of β-catenin [31].

In neuronal cells, upregulation of ATP7A is associated with higher flow of Cu to the secretory pathway and facilitation of Cu delivery to Cu-dependent enzymes dopamine-β-hydroxylate (DBH) and peptidyl-α-monooxygenase (PAM), which are also upregulated during differentiation [8]. Similar events take place in adipocytes, where adipogenesis is associated with increased expression of Atp7a and Aoc3, a Cu-dependent enzyme, which is highly abundant in mature adipocytes and which receives its Cu from Atp7a [21]. However, the timing of Atp7a upregulation in either adipocytes or neuronal cells is not coordinated with the expression of Cu-dependent enzymes, i.e. Atp7a expression peaks much earlier than the increase in Aoc3 or DBH/PAM occur in the respective cells [21]. These results indicate that the early adipogenesis (and neurogenesis) involves changes in Cu distribution, which may affect other processes that are modulated during this time. In neuronal cells, early differentiation steps involve transient lowering of cellular Cu, which coincides with changes in cell morphology [9]. We demonstrate here that in adipocytes, not only abundance of the Atp7a

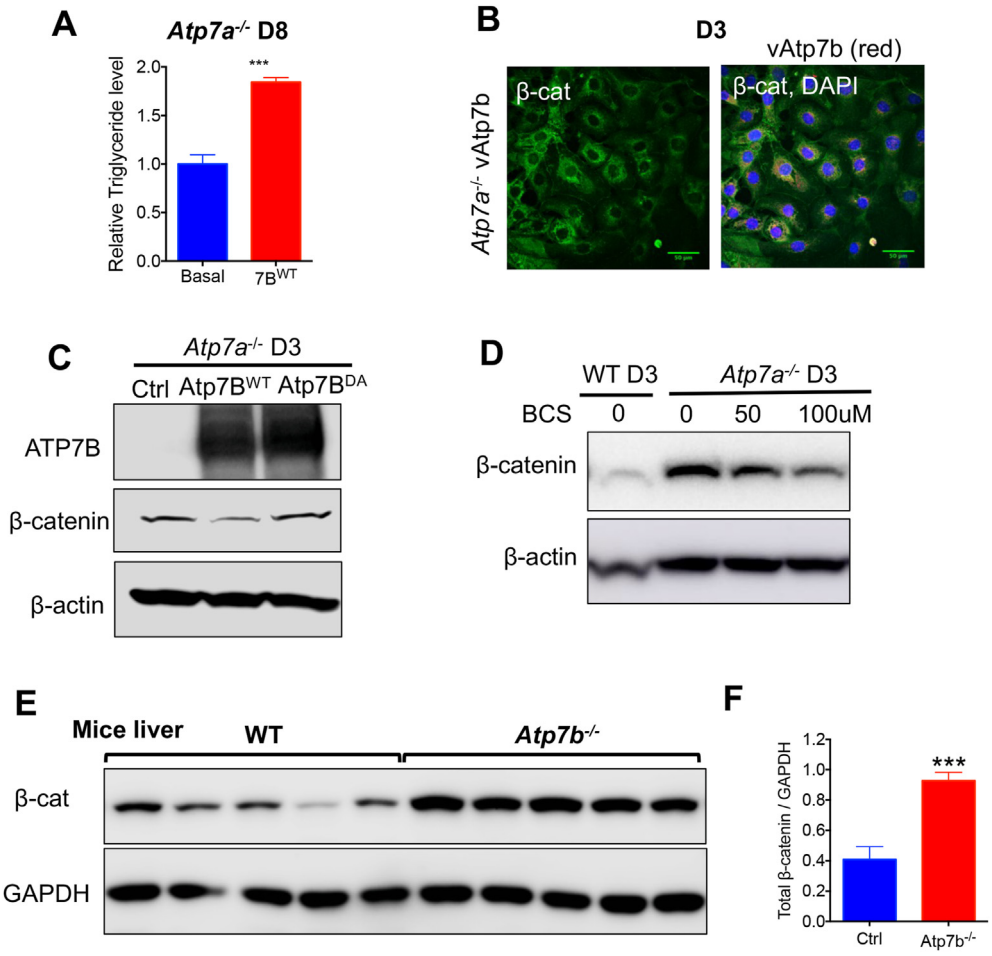

Figure 6: Decrease of Cu normalizes β-catenin degradation, localization, and adipogenesis. (A) Triglyceride levels in differentiated *Atp7a*$^{-/-}$cells in basal medium following expression of WT ATP7B. **(B)** Immunostaining of ATP7B-GFP (red) and β-catenin (green) in *Atp7a*$^{-/-}$ 3T3-L1 cells on day 3. **(C)** Immunoblot of ATP7B and β-catenin in *Atp7a*$^{-/-}$ 3T3-L1 cells on D3 which infected with wild type ATP7B-GFP and DA mutant ATP7B-GFP. **(D)** Immunoblot of β-catenin in WT and *Atp7a*$^{-/-}$ 3T3-L1 cells on D3 incubated with 50 μM or 100 μM Cu chelator BCS since 2 days before and during differentiation. **(E)** Western blot and **(F)** densitometry (right) illustrate elevation of β-catenin in Cu overloaded livers of *Atp7b*$^{-/-}$ mice (n = 5) compared to WT livers. All values represent the mean ± SEM. Student t-test was used for A and F, *** $-$ $p < 0.001$.

protein is increased in the early adipogenesis, but also Atp7a trafficking to the vesicles/plasma membrane, thus lowering cytosolic Cu. These events occur when the transcriptional programs leading to lipid synthesis and cytoskeleton remodeling are being turned on, suggesting that these processes can be sensitive to Cu levels. In fact, in mature adipocytes higher Cu stimulates lipolysis [2], whereas Cu depletion induces lipid accumulation [21]. We propose that Atp7a-mediated transient Cu deficit is beneficial for initiation of lipogenesis and lipid accumulation, and serves as an integral component of the entire differentiation program. The effects of Cu on cytoskeleton and cell morphology were previously observed in 3T3-L1 cells [23], as well as in other cell types [32,33]. Our studies suggest that β-catenin, which coordinates gene transcription and cell adhesion, could be an important factor in the observed morphological changes; however, the role of Cu in adipocyte morphology need to be studied further.

Inactivation of Atp7a results in the elevation of cellular Cu and has dramatic consequences for adipocytes, manifested in inhibition of *Pparγ* expression and low lipid accumulation. Our studies of changes in cell proteome during early steps of adipogenesis reveal that these effects are caused in part by a sustained Wnt/β-catenin signaling. In differentiating 3T3-L1 adipocytes, down-regulation of Wnt/β-catenin signaling, which is inhibitory to adipogenesis [34], coincides with the upregulation of PPARγ, a master regulator of adipogenesis. In 3T3-L1 *Atp7a*$^{-/-}$ cells, elevated Cu causes stabilization of β-catenin and elevated Wnt levels thus prolonging Wnt/β-catenin signaling and inhibiting adipogenesis. Two molecular mechanisms may explain β-catenin stabilization. First, excess Cu is known to cause oxidative stress, and 3T3-L1-*Atp7a*$^{-/-}$ cells were previously shown to have redox misbalance [22,23]. Oxidative stress can cause changes in β-catenin plasma-membrane retention/nuclear distribution and increase expression of Wnt target genes [35]. In addition, elevated Cu was shown to inhibit activity of GSK-3β [36]. GSK-3β mediated phosphorylation is a central event for β-catenin degradation and termination of Wnt/β-catenin signaling. Our study found diminished phosphorylation and increased stabilization of β-catenin, which are consistent with elevated Cu inhibiting Gsk-3β kinase activity. Further studies should determine whether Cu regulates β-catenin directly or through these indirect mechanisms.

Cu excess during early differentiation disrupts lipid accumulation. Previous studies have demonstrated a role for Cu in phosphodiesterase (PDE3) activity, whereby elevated Cu concentrations stimulate PDE3-dependent lipolysis [2]. Defects in lipid accumulation that we observed in *Atp7a*$^{-/-}$ cells can, in part, attribute to this phenomenon. Finally, our finding that elevated Cu prolongs β-catenin stabilization not

only in cultured pre-adipocytes but also *in vivo* in the liver of Wilson disease mouse model offers a new mechanism for Cu-dependent pathologies. This discovery can contribute to a better understanding of the human disorders associated with Cu misbalance.

4. MATERIALS AND METHODS

4.1. Cell lines and culture conditions

3T3-L1 cells were cultured in DMEM (Gibco) supplemented with 10% FBS (Sigma Aldrich) and 1% Penstrep (Gibco). Differentiation of 3T3-L1 cells was done by sequential treatments with first basal medium (BM) for two days after cells reached confluence (day -2), second with basal medium containing IBMX, dexamethasone, insulin, and rosiglitazone (differentiation medium I, DMI) for 3 days (d0-d3), and last with basal medium containing insulin (differentiation medium II, DMII) for 2 days (d3-d5). On day 5, the medium was changed to basal medium for 3—4 days. Cells on day -2 were used as undifferentiated adipocytes, and cells on day 8 or day 9 were used as differentiated mature adipocytes.

4.2. Cell counting for viability and proliferation

3T3-L1 cells were seeded at a density of 15,000 cells/well in 12-well plates in triplicates. On each day, cells were washed and trypsinized with trypsin-EDTA (Gibco). Old medium and trypsin-EDTA were both collected to count for all dead cells. The cell suspensions were then mixed with trypan blue (Gibco) to identify living and dead cells. The cells were then counted using hemacytometers under 10× brightfield microscope.

4.3. Immunoblot analysis

Cells were cultured in 24-well plates, 6-well plates, or 100-mm dishes. Cells or tissue were lysed using 1xRiPA buffer (with EDTA free protease inhibitor cocktail) on ice for 1 h, and debris as well as nuclei were removed by centrifugation at 10000*g* for 15 min. Protein concentration in the resulting cleared lysate was determined by BCA assay. Before electrophoretic separation of proteins, each sample was combined with an equal volume of 2× Laemmlli sample containing 5% β-mercaptoethanol. Proteins were then resolved on 8% Laemmlli SDS-PAGE and transferred to PVDF membrane at 90 V for 90 min using CAPS buffer. Primary antibodies used in immunoblotting were: rabbit anti-ATP7A CT77 (Hycult biotech), mouse monoclonal anti-α-tubulin (Sigma, T8203), mouse anti-β-catenin (BD Biosciences, catalog #610153), rabbit anti-ATP7B (Abcam ab124973), mouse anti-Na/K-ATPase (millipore 05-369), rabbit anti-Phospho-β-catenin (Cell Signaling, catalog #9561), rabbit anti-GSK-3α/β (Cell Signaling, catalog #5676), mouse anti-β-catenin (Santa Cruz, SC-7963). Secondary antibodies were: goat polyclonal anti-mouse IgG HRP-conjugate (Santa Cruz, SC-2005), goat polyclonal anti-rabbit IgG HRP-conjugate (Santa Cruz, SC-2004). All antibodies were used at a dilution of 1:1000.

4.4. Immunostaining of cultured cells

Immunostaining was performed as previously described. Cells were cultured on cover slips in a 12-well plate, fixed with 1:1 Acetone and Methanol solution for 30 s followed by 5 s washing in phosphate buffered saline (PBS), and blocked with 1% (w/v) BSA/1% (w/v) gelatin in PBS. Primary antibodies used in immunoblotting were: rabbit monoclonal anti-mouse and rat anti-ATP7A (Hycult biotech), mouse anti-Syntaxin-6 (BD Transduction Laboratories, 610,636), rabbit polyclonal anti-beta catenin (ab16051), mouse anti-GM-130 (BD Biosciences, 610,822). Secondary antibodies were: goat polyclonal anti-rabbit IgG Alexa488-conjugate (Thermo, A11034), goat polyclonal anti-mouse IgG Alexa555-conjugate (Thermo, A31570). All antibodies were used at a dilution of 1:100. Cells were imaged with a Zeiss LSM710 or Zeiss LSM800. Images were processed with ZEN and ImageJ software.

4.5. Quantitative real-time PCR

Total RNA was isolated from cells with RNEasy kit (Qiagen), and corresponding cDNA pools were synthesized using Fast-Strand cDNA synthesis kit (Roche). RT—PCR was performed with SYBR green (Applied Biosystems) on an ABI 7500 Sequence Detection System (Applied Biosystems). For ddCt analysis, 18 S or NoNo levels were used for normalization. Primers used in this study are listed in supplementary table 1.

4.6. CRISPR/Cas9 genomic edited cell line

Atp7a$^{-/-}$ 3T3-L1 cell line was generated by using CRISPR/Cas9 genomic editing and vector (pEF6/V5-His TOPO TA) expressing Cas9 were as previously described [22]. Briefly, two sgRNA oligos were synthesized for *Atp7a*: *Atp7a* target 1: 5′-GTTTTTCTGTATCCCTGTAATGG-3′; *Atp7a* target 2: 5′-CCTATGCTGTTTGTGTTTATTGC-3′). 3T3-L1 cells were transfected with 2 μg Cas9-sgRNA plasmid using Lipofectamine LTX with Plus Reagent (Life Technologies). Transfected cells were selected by the addition of 3 μg/ml blasticidin in the cell culture medium for two weeks and then diluted into 96-well plates for cell cloning. *Atp7a*-downregulated cell clones were determined by Western blot assay. Mutations in the *Atp7a* gene were further identified through Sanger sequencing.

4.7. X-ray fluorescence microscopy (XFM)

Cultured cells were grown directly onto 4 × 4 mm silicon nitride membranes (SiN, Silson Ltd, Northhampton, England). SiN membranes were sterilized with UV radiation and incubated with 10 μL sterile 0.01% POLY-L-Lysine solution (Sigma—Aldrich, St Louis, MO) at 37 °C. After 30 min, POLY-L-Lysine was removed and 10 μL of cell containing media was added to the membrane. Basal medium was added to the cultures after 15 min at 37 °C. After completion of the experiments, the membranes were rinsed with PBS, fixed with 4% paraformaldehyde for 30 min at 37 °C, rinsed with PBS/isotonic 100 mM ammonium acetate/water, and then air-dried. XFM data were collected on beamline 2-ID-E at the Advanced Photon Source, Argonne National Laboratory (Argonne, IL). SiN membranes were mounted onto kinematic sample holders and target cells were selected using a light microscope (Leica, Buffolo Grove, IL) equipped with a high precision, motorized x, y-stage (Ludl Electronic Products, Hawthorne, NY). Coordinates of target cells were recorded before mounting the sample onto the microprobe stage at the beamline. The microscope coordinates were translated into microprobe coordinates and the cell raster scanned in the x-y plane. The incident X-ray energy was tuned to 10 keV using a Si-monochromator, and the monochromatic beam was focused to 750 × 750 nm using a Fresnel zone plate. The sample was placed at 19° to the incident X-ray beam, and the resulting X-ray fluorescence was collected at 90° using an energy dispersive 4-element detector (Vortex ME-4, SII Nanotechnology, Northridge, CA). Elemental maps were created by extracting, background subtracting, and fitting the fluorescence counts for each element at each point using the program MAPS. The fluorescent photon counts were translated into μg/cm^2 using calibrated X-ray standards (AXO products, Dresden, Germany).

4.8. Triglyceride levels measurement

Cells monolayers cultured in 24 well-plate were washed two times with PBS and lysed with 80 μl 1 × RIPA on ice for 30 min. Cell lysates were vortexed for 30 s, and then triglycerides were quantified calorimetrically as glycerol by use of a commercial enzymatic assay (Infinity

Triglycerides, Fisher Diagnostics). Triglyceride levels were expressed as total triglyceride per well. To compare triglycerides in different cell lines, triglyceride levels were normalized to protein concentration. Cell lysates were centrifuged at 3000*g* for 15 min at 4 °C. Supernatants were used to measure protein concentration using BCA assay.

4.9. Oil red O staining

Cell monolayers cultured in 6 well-plates were washed two times with PBS and then fixed for 2 min with 4% formaldehyde. Cells were then washed two times with water followed by a wash with 60% isopropanol for 5 min. 60% isopropanol was removed completely and cells were left to dry at room temperature. 0.5% Stock Oil Red O (Sigma, O1391) was diluted with water (3:2), filtered through a 0.45 μm filter, and incubated with the fixed dried cells for 2 h at room temperature. Cells were then washed extensively with distilled water, dried, and photographed using a camera.

4.10. Adenoviral infection

Atp7a$^{-/-}$ 3T3-L1 preadipocytes were transduced with AdenoExpress ATP7B-GFP in pAdLOX for adenovirus-mediated protein expression. Briefly, 1% polylysine was added to the serum-free medium prior to the addition of AdenoExpress ATP7B-GFP virus, and then incubated at room temperature for 100 min prior to adding it to the PBS-washed cells. After incubation of the culture being transduced for OptiMEM media (Invitrogen Life Technologies) and then the media were replaced with complete media for 48 h.

4.11. Generation of ATP7A knock-down 3T3-L1 cells

The shRNA pLKO.1-puro plasmids expressed in DH5α *E. coli* strain were purchased from SigmaAldrich (MISSION® shRNA Bacterial Glycerol Stocks, clones nr TRCN0000101810, TRCN0000101812 and TRCN0000101813, products referred as shRNA-10, shRNA-12 and shRNA-13, correspondingly). Lentiviral pMD2.G envelope and psPAX2 packaging plasmids were purchased from Addgene (cat 12,259 and 12,260). HEK293T cell were used as a packaging cell line. Briefly, HEK293T cells were grown to reach 70–80% confluency and were co-transfected with pLKO.1-puro, pMD2.G and psPAX2 plasmids using Lipofectamine® LTX and Plus™ reagent (15,338-100, Invitrogen) following the protocol of the manufacturer. Transfection medium was replaced with fresh medium 6 h after transfection. Virus packaging was confirmed by the presence of virus plaques. Lentivirus particles containing medium was harvested 48 h after transfection and stored in −80 °C until transduction of 3T3-L1 cells. Before transduction, virus containing medium was slowly thawed on ice, diluted to obtain proper MOI and added to 3T3-L1 preadipocytes (1×10^9 particles/ml). Transduction medium was replaced with complete growth medium 24 h after infection. pLKO.1-puro plasmids expressing 3T3-L1 cells were selected using puromycin. The shRNA constructs sequences were: shRNA-10: 5′CCGGCGTGCAAGGATCT-TATGTCAACTCGAGTTGACATAA-GATCCTTGCACGTTTTTG3'; shRNA-12:5′CCGGCGGAC-CATTGAACAGCA-GATTCTCGAGAATCTGCTGTTCAATGGTCCGTTTTTG3'; shRNA-13: 5′CC-GGCCCGAGTGATAGCAGAGTTTACTCGAGTAAACTCTGCTATCACTCGGGTT TTTG3'.

4.12. Mass spectrometry analysis

Samples were prepared as described previously [21]. Briefly, Wild type, *Atp7a*$^{-/-}$, BSC treated *Atp7a*$^{-/-}$ 3T3-L1 cells at confluent stage (day 0) or 3 days stimulated with differentiation medium I, DMI (IBMX, dexamethasone, insulin, and rosiglitazone) day 3 were cultured and washed three times with cold phosphate-buffered saline (PBS). Extraction solution consisted of 55 mM iodoacetamide in buffer (100 mM pH 8.5 Tris-HCl buffer, 4% SDS) was added to cells to alkylate free cysteine thiols upon lysis per each condition. Cells were scraped immediately on ice and sonicated. All samples were centrifuged at 16,000 g for 5 min at 4 °C. Supernatants were then incubated in the dark at a shaker with 1400 rpm for 1 h at room temperature. Protein concentration was determined by BCA assay. 80 μg proteins from each sample were treated with 70 mM DTT and incubated at room temperature (24 °C) for 45 min to reversibly reduce their oxidise thiols. Samples were added one volume of 50 mM ammonium bicarbonate solution (pH 7.0). Newly generated free thiols were subsequently alkylated using 80 mM NEM. Finally proteins were then precipitated using trichloroacetic acid (TCA) and used to perform samples for mass spectrum.

Approximately 1 μg of each fraction, (calculated based on the original amount of total protein) was analyzed by liquid chromatography interfaced with tandem mass spectrometry (LC/MS-MS) using a Thermo Easy-LC interfaced with a Fusion (www.thermofisher.com), and isotopically resolved masses in precursor (MS) and fragmentation (MS/MS) spectra were extracted from raw MS data without deconvolution and with deconvolution using Xtract or MS2 Processor in Proteome Discoverer (PD) software (v1.4, Thermo Scientific) as described before [21]. Protein quantification is based on the normalized median ratio of all spectra of tagged peptides from the same protein [37].

4.13. Bioinformatic analysis

Multivariate statistics and associated graphics were performed in R version 3.4.1. Fold change of protein levels were analyzed using limma package. Heat maps were drawn using the heatmap.2 function found in the ggplots package. The associations between altered proteins and pathways were evaluated using the Ingenuity Pathways Analysis software (Ingenuity Systems, www.ingenuity.com). Differentially expressed proteins and their corresponding expression values were loaded into the software and mapped to associated pathway functions that were generated from existing literature from the Ingenuity Systems Knowledge Base.

4.14. Mice husbandry and tissue collection

Animals were housed at the Johns Hopkins University, School of Medicine (JHU SOM) animal care facility, and the studies followed the National Institutes of Health guidelines. Animal protocols were approved by the Institutional Animal Care and Use Committee (protocol number M017M385). Atp7b KO (*Atp7b*$^{-/-}$) and littermate WT mice of C57BL/6 × 129S6/SvEv background (described in [38]) were fed with the standard pellet chow. At 20 weeks after birth, mice were euthanized and dissected to take different tissues. Liver samples were used for immunoblot analysis. Tissues were flash-frozen and stored at −80 °C until protein extraction.

4.15. Statistical analysis

Statistical analysis was performed using Prism software version 6.0b (GraphPad Software). Two-tailed Student's t-tests, One-way ANOVA or Two-way ANOVA were used when appropriate. All data in the figures are shown as the mean ± SEM. A p value of less than 0.05 was considered significant, and ns stands for $p > 0.05$, * - $p < 0.05$, ** - $p < 0.01$, *** - $p < 0.001$, **** - $p < 0.0001$.

CREDIT AUTHORSHIP CONTRIBUTION STATEMENT

H. Yang: Conceptualization, Data curation, Formal analysis, Investigation, Methodology, Validation, Writing — original draft, Writing — review

& editing. **E. Kabin:** Data curation, Formal analysis, Investigation, Writing — review & editing. **Y. Dong:** Data curation, Formal analysis, Investigation, Writing — review & editing. **X. Zhang:** Formal analysis, Investigation. **M. Ralle:** Formal analysis, Investigation, Methodology. **S. Lutsenko:** Formal analysis, Funding acquisition, Project administration, Supervision, Visualization, Writing — review & editing.

ACKNOWLEDGEMENTS

This work was supported by the NIDDK and OD grant 2 R01 DK071865-14A1. We thank Dr. S. Jayakanthan for providing the adenovirus encoding ATP7B and Dr. W.G. Wong for help and advice with the initial stages of this project. The analysis of proteomes was done at the Johns Hopkins Mass Spectrometry and Proteomics Core supported by the Johns Hopkins Institute for Clinical and Translational Research/Translational Science Cores (NCATS center grant UL1 TR003098); the JHU Sidney Kimmel Comprehensive Cancer Center (NCI center grant P30 CA006973) and the Hopkins Digestive Diseases Basic and Translational Research Core Center (NIDDK center grant P30 DK089502). Grants from Dora Plus 1.2 and Kristjan Jaak Scholarship Programmes were awarded by Archimedes Foundation (Education and Youth Board, Estonia) to E.K.

DECLARATION OF COMPETING INTEREST

The authors declare no any financial and personal relationships with other people or organizations that could inappropriately influence this work.

DATA AVAILABILITY

Data will be made available on request.

APPENDIX A. SUPPLEMENTARY DATA

Supplementary data to this article can be found online at https://doi.org/10.1016/j.molmet.2024.101872.

REFERENCES

[1] Tsang T, Davis CI, Brady DC. Copper biology. Curr Biol 2021;31:R421—7. https://doi.org/10.1016/j.cub.2021.03.054.

[2] Krishnamoorthy L, Cotruvo JA, Chan J, Kaluarachchi H, Muchenditsi A, Pendyala VS, et al. Copper regulates cyclic-AMP-dependent lipolysis. Nat Chem Biol 2016;12:586—92. https://doi.org/10.1038/nchembio.2098.

[3] Tsang T, Posimo JM, Gudiel AA, Cicchini M, Feldser DM, Brady DC. Copper is an essential regulator of the autophagic kinases ULK1/2 to drive lung adenocarcinoma. Nat Cell Biol 2020;22:412—24. https://doi.org/10.1038/s41556-020-0481-4.

[4] Chojnowski JE, Li R, Tsang T, Alfaran FH, Dick A, Cocklin S, et al. Copper modulates the catalytic activity of protein kinase CK2. Front Mol Biosci 2022;9.

[5] Tsvetkov P, Coy S, Petrova B, Dreishpoon M, Verma A, Abdusamad M, et al. Copper induces cell death by targeting lipoylated TCA cycle proteins. Science 2022;375:1254—61. https://doi.org/10.1126/science.abf0529.

[6] Lutsenko S. Dynamic and cell-specific transport networks for intracellular copper ions. J Cell Sci 2021;134:jcs240523. https://doi.org/10.1242/jcs.240523.

[7] Hordyjewska A, Popiołek Ł, Kocot J. The many "faces" of copper in medicine and treatment. Biometals 2014;27:611—21. https://doi.org/10.1007/s10534-014-9736-5.

[8] Hatori Y, Yan Y, Schmidt K, Furukawa E, Hasan NM, Yang N, et al. Neuronal differentiation is associated with a redox-regulated increase of copper flow to the secretory pathway. Nat Commun 2016;7:10640. https://doi.org/10.1038/ncomms10640.

[9] McCann CJ, Hasan NM, Padilla-Benavides T, Roy S, Lutsenko S. Heterogeneous nuclear ribonucleoprotein hnRNPA2/B1 regulates the abundance of the copper-transporter ATP7A in an isoform-dependent manner. Front Mol Biosci 2022;9.

[10] El Meskini R, Crabtree KL, Cline LB, Mains RE, Eipper BA, Ronnett GV. ATP7A (Menkes protein) functions in axonal targeting and synaptogenesis. Mol Cell Neurosci 2007;34:409—21. https://doi.org/10.1016/j.mcn.2006.11.018.

[11] Vest KE, Paskavitz AL, Lee JB, Padilla-Benavides T. Dynamic changes in copper homeostasis and post-transcriptional regulation of Atp7a during myogenic differentiation. Metallomics 2018;10:309—22. https://doi.org/10.1039/c7mt00324b.

[12] Herman S, Lipiński P, Ogórek M, Starzyński R, Grzmil P, Bednarz A, et al. Molecular regulation of copper homeostasis in the male gonad during the process of spermatogenesis. Int J Mol Sci 2020;21. https://doi.org/10.3390/ijms21239053.

[13] Finney L, Mandava S, Ursos L, Zhang W, Rodi D, Vogt S, et al. X-ray fluorescence microscopy reveals large-scale relocalization and extracellular translocation of cellular copper during angiogenesis. Proc Natl Acad Sci USA 2007;104:2247—52. https://doi.org/10.1073/pnas.0607238104.

[14] Lei L, Sui X, Li F. Effect of dietary copper addition on lipid metabolism in rabbits. Food Nutr Res 2017;61.

[15] Yang H, Liu CN, Wolf RM, Ralle M, Dev S, Pierson H, et al. Obesity is associated with copper elevation in serum and tissues. Metallomics 2019;11:1363—71. https://doi.org/10.1039/c9mt00148d.

[16] Chen M, Li R, Yin W, Wang T, Kang YJ. Copper promotes migration of adipose-derived stem cells by enhancing vimentin-Ser39 phosphorylation. Exp Cell Res 2020;388:111859. https://doi.org/10.1016/j.yexcr.2020.111859.

[17] Tao C, Wang Y, Zhao Y, Pan J, Fan Y, Liang X, et al. Adipocyte-specific disruption of ATPase copper transporting α in mice accelerates lipoatrophy. Diabetologia 2019;62:2340—53. https://doi.org/10.1007/s00125-019-4966-2.

[18] Ma H, Li Y-n, Song L, Liu R, Li X, Shang Q, et al. Macrophages inhibit adipogenic differentiation of adipose tissue derived mesenchymal stem/stromal cells by producing pro-inflammatory cytokines. Cell Biosci 2020;10:88. https://doi.org/10.1186/s13578-020-00450-y.

[19] Bagchi DP, MacDougald OA. Wnt signaling: from mesenchymal cell fate to lipogenesis and other mature adipocyte functions. Diabetes 2021;70:1419—30. https://doi.org/10.2337/dbi20-0015.

[20] Zebisch K, Voigt V, Wabitsch M, Brandsch M. Protocol for effective differentiation of 3T3-L1 cells to adipocytes. Anal Biochem 2012;425:88—90. https://doi.org/10.1016/j.ab.2012.03.005.

[21] Yang H, Ralle M, Wolfgang MJ, Dhawan N, Burkhead JL, Rodriguez S, et al. Copper-dependent amino oxidase 3 governs selection of metabolic fuels in adipocytes. PLoS Biol 2018;16:e2006519. https://doi.org/10.1371/journal.pbio.2006519.

[22] Bhattacharjee A, Yang H, Duffy M, Robinson E, Conrad-Antoville A, Lu YW, et al. The activity of menkes disease protein ATP7A is essential for redox balance in mitochondria. 2016.

[23] Kabin E, Dong Y, Roy S, Smirnova J, Smith JW, Ralle M, et al. α-lipoic acid ameliorates consequences of copper overload by up-regulating selenoproteins and decreasing redox misbalance. Proc Natl Acad Sci USA 2023;120:e2305961120. https://doi.org/10.1073/pnas.2305961120.

[24] Yang L, McRae R, Henary MM, Patel R, Lai B, Vogt S, et al. Imaging of the intracellular topography of copper with a fluorescent sensor and by synchrotron x-ray fluorescence microscopy. Proc Natl Acad Sci USA 2005;102:11179—84. https://doi.org/10.1073/pnas.0406547102.

[25] Perrin L, Roudeau S, Carmona A, Domart F, Petersen JD, Bohic S, et al. Zinc and copper effects on stability of tubulin and actin networks in dendrites and spines of hippocampal neurons. ACS Chem Neurosci 2017;8:1490—9. https://doi.org/10.1021/acschemneuro.6b00452.

[26] Tanaka T, Yoshida N, Kishimoto T, Akira S. Defective adipocyte differentiation in mice lacking the C/EBPβ and/or C/EBPδ gene. EMBO J 1997;16:7432—43. https://doi.org/10.1093/emboj/16.24.7432.

[27] Ross SE, Hemati N, Longo KA, Bennett CN, Lucas PC, Erickson RL, et al. Inhibition of adipogenesis by Wnt signaling. Science 2000;289:950—3. https://doi.org/10.1126/science.289.5481.950.

[28] Cawthorn WP, Bree AJ, Yao Y, Du B, Hemati N, Martinez-Santibañez G, et al. Wnt6, Wnt10a and Wnt10b inhibit adipogenesis and stimulate osteoblastogenesis through a β-catenin-dependent mechanism. Bone 2012;50:477—89. https://doi.org/10.1016/j.bone.2011.08.010.

[29] Ha N-C, Tonozuka T, Stamos JL, Choi H-J, Weis WI. Mechanism of phosphorylation-dependent binding of APC to β-catenin and its role in β-catenin degradation. Mol Cell 2004;15:511—21. https://doi.org/10.1016/j.molcel.2004.08.010.

[30] Muchenditsi A, Yang H, Hamilton JP, Koganti L, Housseau F, Aronov L, et al. Targeted inactivation of copper transporter Atp7b in hepatocytes causes liver steatosis and obesity in mice. Am J Physiol Gastrointest Liver Physiol 2017;313:G39—49. https://doi.org/10.1152/ajpgi.00312.2016.

[31] Liu D-X, Hao S-L, Yang W-X. Crosstalk between β-CATENIN-mediated cell adhesion and the WNT signaling pathway. DNA Cell Biol 2022;42:1—13. https://doi.org/10.1089/dna.2022.0424.

[32] Chen X, Hu J-G, Huang Y, Li S, Li S-f, Wang M, et al. Copper promotes the migration of bone marrow mesenchymal stem cells via Rnd3-dependent cytoskeleton remodeling. J Cell Physiol 2020;235:221—31.

[33] Milewska M, Burdzińska A, Zielniok K, Siennicka K, Struzik S, Zielenkiewicz P, et al. Copper does not induce tenogenic differentiation but promotes migration and increases lysyl oxidase activity in adipose-derived mesenchymal stromal cells. Stem Cell Int 2020;2020:9123281. https://doi.org/10.1155/2020/9123281.

[34] de Winter TJJ, Nusse R. Running against the Wnt: how Wnt/β-catenin suppresses adipogenesis. Front Cell Dev Biol 2021;9.

[35] Funato Y, Michiue T, Asashima M, Miki H. The thioredoxin-related redox-regulating protein nucleoredoxin inhibits Wnt—β-catenin signalling through Dishevelled. Nat Cell Biol 2006;8:501—8. https://doi.org/10.1038/ncb1405.

[36] Hickey JL, Crouch PJ, Mey S, Caragounis A, White JM, White AR, et al. Copper(ii) complexes of hybrid hydroxyquinoline-thiosemicarbazone ligands: GSK3β inhibition due to intracellular delivery of copper. Dalton Trans 2011;40:1338—47. https://doi.org/10.1039/C0DT01176B.

[37] Herbrich SM, Cole RN, West Jr KP, Schulze K, Yager JD, Groopman JD, et al. Statistical inference from multiple iTRAQ experiments without using common reference standards. J Proteome Res 2013;12:594—604. https://doi.org/10.1021/pr300624g.

[38] Buiakova OI, Xu J Fau - Lutsenko S, Lutsenko S Fau - Zeitlin S, Zeitlin S Fau - Das K, Das K, Fau - Das S, et al. Null mutation of the murine ATP7B (Wilson disease) gene results in intracellular copper accumulation and late-onset hepatic nodular transformation. Hum Mol Genet. 1999 Sep;8:1665—71. https://doi.org/10.1093/hmg/8.9.1665.

